(NASA-CR-174296) RESEARCH PROGRAM TO STUDY TRANSITION METAL TRIMERS AND EMBEDDED CLUSTERS Semiannual Progress Report, 1 Jul. 1984 - 31 Dec. 1984 (Eloret Corp.) 55 p HC A04/MF A01

N85-.7093

CSCL 11F G3/26

Unclas 13479

Semiannual Progress Report

for

Theoretical Research Program To Study Transition Metal Trimers and Embedded Clusters

July 1,1984 - December 31,1984

Cooperative Agreement No: NCC 2-096

Period of award: July 1, 1984 - June 30, 1987

Principal Investigator: Stephen P. Walch

Eloret Institute
1178 Maraschino Drive
Sunnyvale, Ca. 94087

The objective of this research is to study small transition metal clusters at a high level of approximation i.e. including all the valence electrons in the calculation and also including extensive electron correlation. A major goal of this study is to understand the electronic structure of these small metal clusters and by comparison of dimers, trimers and possibly higher clusters to extrapolate the information obtained to provide insights into the electronic structure of bulk transition metals. Small metal clusters are currently of considerable experimental interest and some information is currently becomming available both from matrix ESR studies and from gas phase spectroscopy. Collaboration between theorists and experimentalists is thus expected to be especially profitable at this time since there is some experimental information which can serve to guide the theoretical work. It should be pointed out here that transition metal molecules have been difficult for both theory and experiment and a close collaboration between theory and experiment is likely to lead to a deeper understanding than would be obtained by either approach alone.

These studies are expected to be applied in several areas. One area of current interest is the reactivity of small metal clusters. As an example Smalley et. al. have studied the reactivity of H_2 with Nb clusters and find that Nb atom and Nb_2 are unreactive to H_2 while Nb_3 is reactive to H_2. Similarly, several groups have observed that transition metals form compounds of specific stochiometry with O or H atoms. These observations are relevant to understanding the catalytic properties of small clusters but the thoretical basis for understanding these observations does not exist because of the very limited understanding of the electronic structure of these metal clusters. In this area theory may well be able to provide results

more rapidly than experiment. For example for the Nb_2 molecule theory is able to study the potential curves as easily as for the V_2 molecule but the spectroscopic analysis for Nb_2 is much more difficult than for V_2 and has not been possible to date. Similarly it should be possible to study Nb_3 computationally and a comparison of the electronic structure of Nb_2 and Nb_3 should provide some insight into why one is reactive to H_2 while the other is not.

A second area of application of these studies is in understanding the interaction of bulk metals with hydrogen i.e. hydrogen embrittlement. Here studies had been carried out earlier of the potential function for a single hydrogen atom interior to BCC iron using a one-electron ECP which replaces the $3d^7$ Fe atom configuration as well as the Ar core i.e. only a single 4s electron is left on each iron atom (Walch. Work carried out under NCC2-148). Here the plan is to place a small cluster of iron atoms with the 3d electrons included inside a larger cluster with the remaining atoms treated at the one-electron ECP level. This approach would permit studying features which would not be treated reliably by the one-electron ECP approach such as the formation of an FeH_2 phase where metal 3d electrons may be involved in the bonding.

In the first six months of this grant calculations have been carried out for the the Y_2, Nb_2, and Mo_2 molecules thus extending the earlier studies of the first row transition metal dimers to elements of the second transition row. These studies show that the second transition row elements form stronger nd bonds due to i) a larger 4d to 5s orbital size ratio as compared to the 3d to 4s orbital size ratio for the first transition row and ii) smaller nd exchange interactions for the second transition row as compared to the

first transition row. Calculations were also carried out for the TiV molecule which was of experimental interest since it has been observed via ESR in a matrix. Here the calculations confirmed the $^4\Sigma^-$ ground state symmetry which had been deduced from the ESR experiments. The details of this work along with the previous work on first row transition metal dimers have been presented in a paper which is included as an appendix to this report and will not be discussed further here.

In addition to the studies of diatomic molecules presented above studies are currently in progress for selected transition metal trimers. Currently the Ca_3, Sc_3, Y_3, and Cu_3 molecules are being studied.

For the Cu_3 molecule all-electron studies are being carried out for the ^2E state arising from three $4s^13d^{10}$ Cu atoms. These studies are single configuration SCF plus configuration interaction (CI) calculations with an [8s6p3d] basis set. From studies on Cu_2 one expects these calculations to lead to somewhat too long Cu-Cu bond lengths due to a combination of relativistic and size consistency effects. However, these calculations should lead to accurate relative energetics for the various geometric isomers of Cu_3. Two major structural possibilities exist here, linear and near equilateral triangle. Because the equilateral triangle form of Cu_3 is a ^2E state one expects a Jahn-Teller distortion leading to $^2A_1$ and $^2B_2$ states in C_{2v} symmetry. For the near equilateral triangle geometries the Cu-Cu distance was first optimized for equilateral triangle geometries leading to an optimal Cu-Cu distance of 4.60 a_0. The $^2A_1$ and $^2B_2$ states were then studied as a function of Cu-Cu-Cu angle with two sides fixed at 4.60 a_0. The resulting curves are shown in Fig. 1 where one sees that the ^2E state is a maximum on the potential surface while the $^2A_1$ state has an acute angle geometry

Fig. 1 CU3, DOUBLET E STATE, SCF/CI

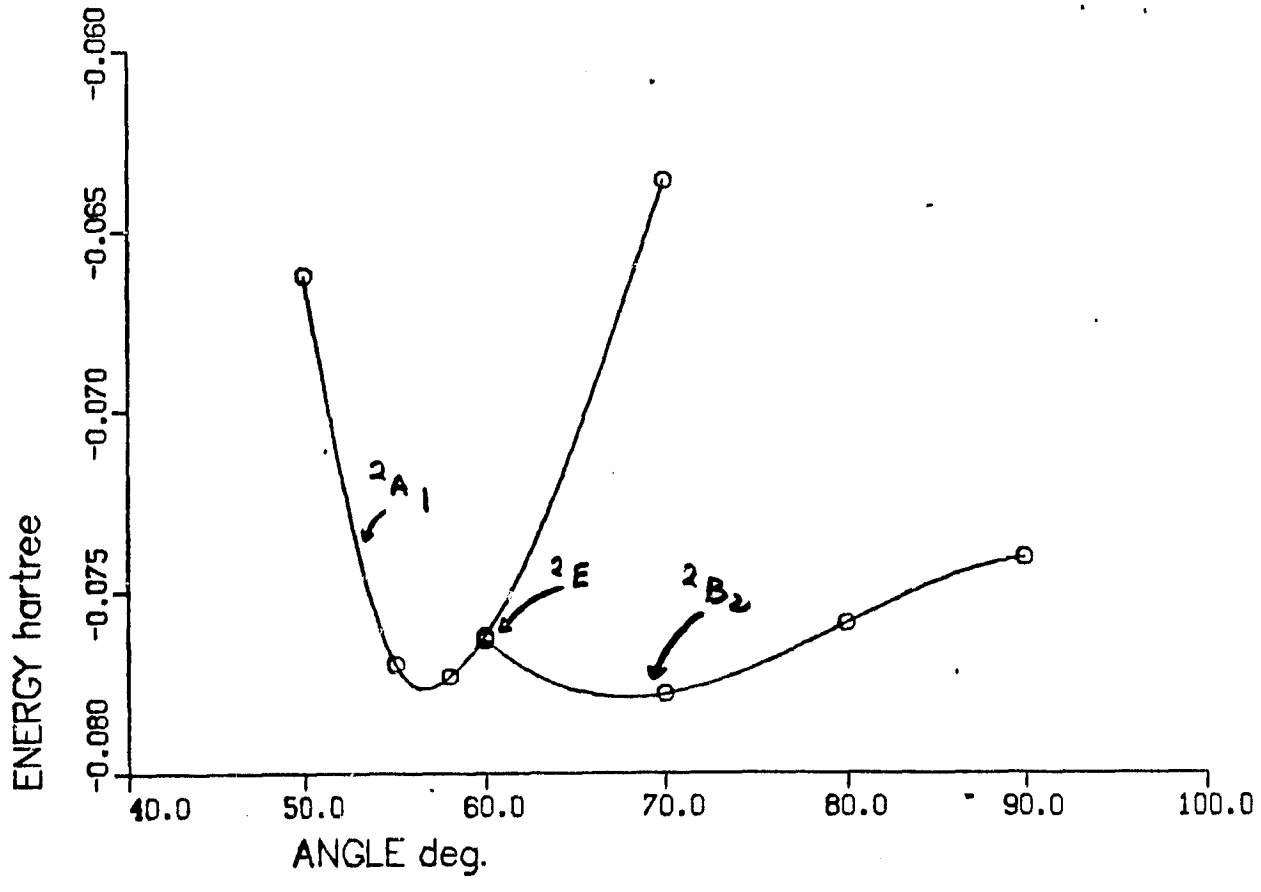

and the $^2B_2$ state has an obtuse angle geometry. The details of the potential surface interconnecting these isomers are under study. One possibility is that the $^2B_2$ state is one of three equivalent minima while the $^2A_1$ state is one of three equivalent saddle points. The calculations do indicate that the linear isomer of Cu_3 is at least 0.2 eV higher than the equilateral triangle geometries. This result is consistent with the interpretation of the spectroscopic results of Smalley et. al. where it is concluded that the ground state of Cu_3 is a strongly Jahn-Teller distorted molecule.

Calculations are also being carried out for Sc_3 and Y_3. These systems were selected for study because of the ESR studies of Weltner et.al. which establish that the ground state of Sc_3 is a doublet state with equivalent Sc atoms while Y_3 is a doublet state with inequivalent Y atoms. The calculations are made tractable by the use of an ECP to replace the Ne core for Sc and the Ar core for Y. This leaves the ns and np core levels in the valence space and is more reliable than had these levels been incorporated into the ECP. The ECPs were developed by Wadt and Hay and have been tested against all-electron calculations for Sc_2, Y_2, and Nb_2.

The calculations are CASSCF calculations with the (n+1)s and nd in the active space and use a [4s4p3d1f] valence basis set. With this size active space for Sc_3 there are a small enough number of electrons that we can allow the MCSCF procedure to scan all possible states. The first encouraging result is that the doublet states are lower than the high spin states and the wavefunctions show very definite indications of 3d bonding. Three doublet states have been studied. The dominant configurations for these states are:

$^2A'\ 4s\sigma a_1'^2\ 4s\sigma e'^4\ 3d\sigma a_1'^1\ 3d\pi a_1''^2$

$^2A''$ $4s\sigma a_1'^2$ $4s\sigma e'^4$ $3d\sigma a_1'^2$ $3d\pi a_1''^1$

^2E $4s\sigma a_1'^2$ $4s\sigma e'^3$ $3d\sigma a_1'^2$ $3d\pi a_1''^2$

Figure 2 shows the energy of the $^2A'$, the $^2A''$ and the ^2E states as a function of the Sc-Sc distance for equilateral triangle geometries. The ^2E state dissociates to two ground state atoms and one excited state atom while the other two states dissociate to three ground state atoms. The CASSCF curve for ^2E shows a well near R Sc-Sc of 5.5 au,while the $^2A''$ shows only repulsive behavior as far out as 5.75 au. Preliminary contracted CI results indicate that the $^2A'$ and $^2A''$ states are bound by about 0.75 eV at R Sc-Sc of about 5.5 a_0 and also one expects the ^2E state to be bound at a geometry near the CASSCF geometry. However,the corresponding contracted CI calculation for this state may be beyond present computational capabilities.

The state that seems most in line with the ESR results is the $^2A'$ or $^2A''$ state since these states would not Jahn-Teiler distort and have almost no 4s character in the singly occupied orbital. Also there is a very low-lying state observed by Moskovitts et.al. which is consistent with the small separation between the $^2A'$ and $^2A''$ states.

If the true ground state is $^2A'$ or $^2A''$ that implies some real differences between Sc_2 and Sc_3 since Sc_2 has a ground state which arises by 4s to 3d promotion while the $^2A'$ state is bonding largely because of 4s to 4p promotion. The populations here are 4s=4.50, 4p=1.21,3d=3.25,and 4f=0.04 for the $^2A'$ state at R Sc-Sc of 5.5 a_0.

Calculations have also been carried out for Y_3 at the CASSCF level. Here the lowest configuration at the CASSCF level for equilateral triangle geometries is the $^2A'$ state.(See Figure 3.) This state would not be consistent with the nonequivalent Y atoms observed in the ESR spectrum.

Fig. 2 SC3,CASSCF (equilateral triangle geometries)

Fig. 3 Y3, CASSCF (equilateral triangle geometries)

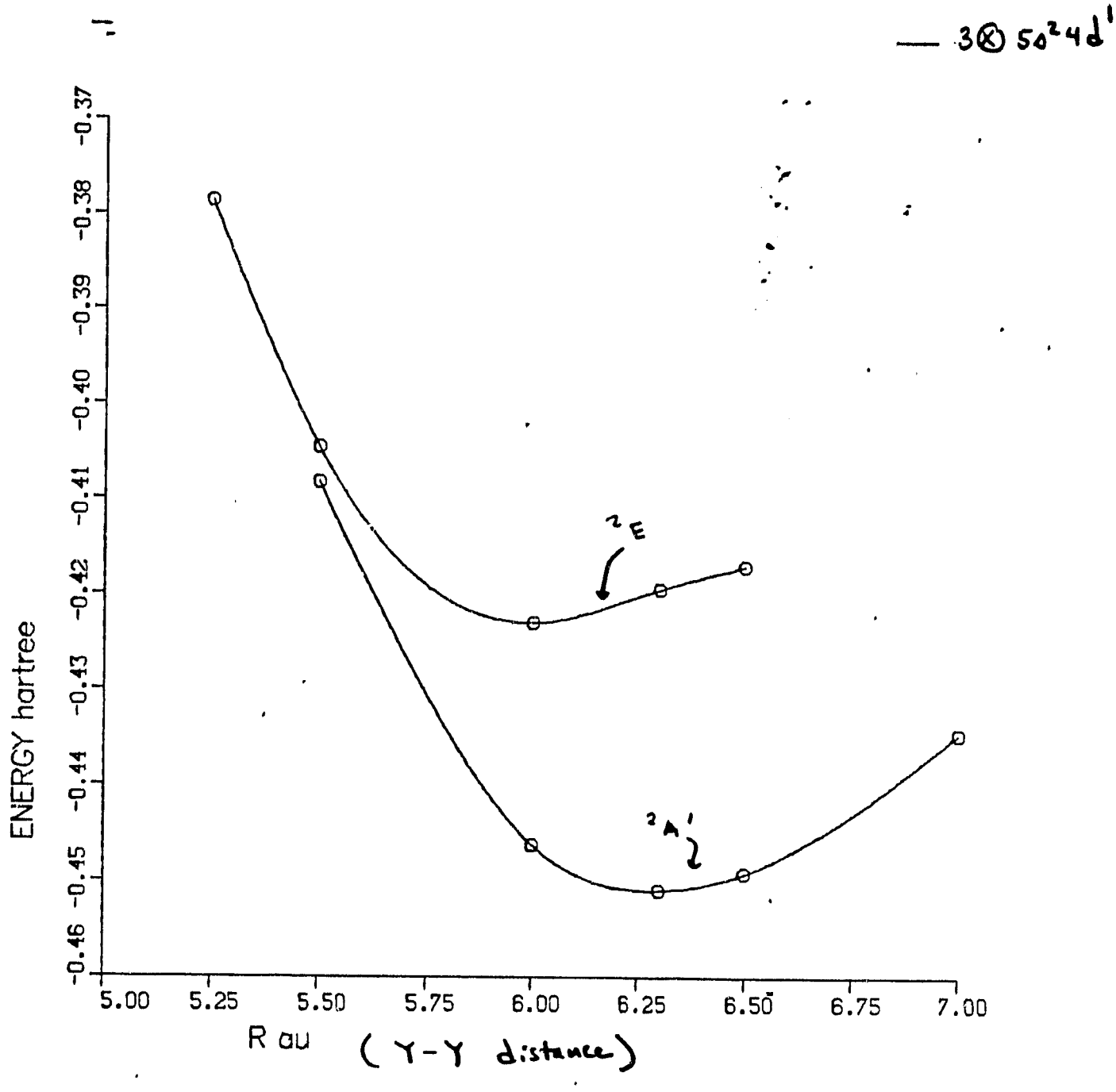

However, for linear geometries there is a low-lying $^2\Sigma^+$ state which could be consistent with the non-equivalent Y atoms. The populations for Y_3 are 5s=3.69,5p=2.25,4d=2.99, and 4f=0.06 for the $^2A'$ state at R Y-Y=6.3 a_0 which is the minimum energy for equilateral triangle geometries. The much larger valence p population here is consistent with a lower s to p promotion energy for the Y atom as compared to the Sc atom and may be consistent with a significant change of geometry between Sc_3 and Y_3. This point requires further study.

Appendix A. The following manuscript describes the calculations for transition metal dimers.

Theoretical Studies of Transition Metal Dimers

Stephen P. Walch†
Eloret Institute
Sunnyvale, CA 94087
and
Charles W. Bauschlicher, Jr
NASA Ames Research Center
Moffett Field, CA 94035

Abstract

The results of CASSCF calculations are presented for the Sc_2, Ti_2, V_2, Cr_2, Cu_2, TiV, Y_2, Nb_2, and Mo_2 molecules. CASSCF/CI calculations were also carried out for Sc_2, Ti_2, Cu_2, and Y_2. The CASSCF procedure is found to generally provide reliable R_e and ω_e values. However, D_e values are systematically underestimated at the CASSCF level; the worst case is Cr_2 where the CASSCF curve is not bound although a shoulder is observed in the region near the experimental R_e. The CASSCF procedure is shown to provide a consistent set of calculations for these molecules from which trends and a simple qualitative picture of the electronic structure may be derived. These calculations confirm the $^5\Sigma_g^-$ ground state of Sc_2 and the $^4\Sigma^-$ ground state of TiV and lead to predictions for other molecules in this series. So far only the $^3\Sigma_g^-$ ground state symmetry and the bond length of V_2 have been confirmed by experiment.

†Mailing address: NASA Ames Research Center, Moffett Field, CA 94035

I. Introduction

Transition metals and transition metal(TM) compounds are currently of considerable interest because of their relevance to catalysis and to materials science problems such as hydrogen embrittlement and crack propagation in metals. In spite of such interest, progress in understanding the chemistry of TM molecules has been slow due to both experimental and theoretical difficulties. For a review of the current state of both theory and experiment for TM molecules the reader is referred to the review article by Weltner and Van Zee[1]. Recent progress in the experimental characterization of TM molecules has come from both matrix isolation and gas phase spectroscopic approaches, while progress in the theoretical treatment of TM molecules has occurred as a result of improved methods of treating electron correlation. These improvements in part involve more efficient computational methods such as improved MCSCF[2], CASSCF[3], and direct CI[4] techniques but also qualitative ideas such as the GVB[5] method have provided a conceptual framework for understanding electron correlation effects in these molecules.

A dramatic example of the importance of electron correlation for transition metal compounds is given by the NiCO $X\,^1\Sigma^+$ state. This state is unbound by 2.6eV at the SCF level, while the triplet states are only slightly repulsive [6].. The Mulliken populations for the triplet states show a 3d population of 9, while the $^1\Sigma^+$ state has a 3d population near 10. If an MCSCF approach is used, the 3d population for the triplet states is only slightly changed, but the 3d population for the $^1\Sigma^+$ state is qualitatively different, 9.5. This arises because of the mixing of the Ni $4s^13d^9$ (^1D) and $3d^{10}$ (^1S) states, and the $^1\Sigma^+$ state is now the ground state of NiCO.

It would take a very large CI to over come the $3d^{10}$ bias of the SCF reference. In this case, the CASSCF wavefunction yields results in remarkable agreement with a multi-reference singles and doubles CI calculation [6] and a D_e of 1.3eV which is quite consistent with experiment (1.3 ± 0.6 eV [7]).

MCSCF treatments do not always yield results as good as those obtained for NiCO but they usually do represent a major improvement over SCF results. For an especially difficult case, the Cr_2 molecule, SCF leads to a potential curve which is unbound with respect to the SCF atoms by 10 eV in the region near the experimental R_e. An MCSCF treatment shows the outer well arising from the 4s-4s bonding but is still unbound by 1.4 eV in the region near R_e where one expects multiple 3d-3d bonds [8,9]. While this might appear to be a major failing of the MCSCF approach, if Cr_2 is compared to Mo_2 [8] and V_2 [9], both of which are bound at the MCSCF level, useful information about the nature of the bonding in Cr_2 can be inferred. Thus, unlike the chemistry of the first two rows of the periodic table, where computational chemistry is achieving accuracy comparable with experiment, for some transition metal compounds only qualitative accuracy is possible.However, so little is known about many of these systems that even qualitative information can contribute to a basic understanding of the chemistry. This is somewhat pessimistic since the MCSCF procedure does lead to good R_e and ω_e values for many of the TM dimers even if the binding energies are systematically underestimated and can treat states arising from the same occupation to very similar accuracy thus in these cases T_e values should be good. When comparing very different states, sometimes a combination of theory and experiment can combine to resolve a question.

For example for Ti_2 theory can calculate the R_e and ω_e of the low-lying $^1\Sigma_g^+$ and $^7\Sigma_u^+$ states but can not clearly establish which is the ground state. However, combining the calculated results with the experimental ω_e leads to a clear assignment of a $^1\Sigma_g^+$ ground state and provides new information about the chemistry.

Many people have investigated individual transition metal dimers (see review article of Weltner and Van Zee [1]). However, as noted for Cr_2, a consistent set of calculations can reveal trends which greatly contribute to the understanding. Goodgame and Goddard have considered Cr_2 and Mo_2 [8], Shim and co-workers [10-11] have considered several transition metal dimers for those metal atoms with more than half filled nd shells, and these authors have considered many of the dimers for those metal atoms with less than half filled nd shells where strong nd-nd bonding is common. In this article we summarize our previous work, report on several unpublished systems and describe the trends for the bonding in the transition metal dimers on the left side of the first two transition metal rows. Here we concentrate on the CASSCF results since this level of calculation is possible for all the systems and provides a useful qualitative understanding. However, for some systems we also are able to carry out multi-reference singles and doubles CI(MRSDCI) calculations using the CASSCF orbitals and these calculations serve to calibrate the CASSCF approach. For other systems, such as Cr_2, the CASSCF+MRSDCI approach is not possible. This has led to several attempts to understand the bonding using even more qualitative approaches [12-14]. These include the extended MCSCF approaches [12-13] and approaches based upon physical arguments [14].

Section II describes some trends for the transition-metal atoms which

are important for understanding the bonding of the TM dimers and also discusses qualitative features of the bonding in the TM dimers. Section III discusses the technical details of the calculations. Section IV discusses the potential curves and spectroscopic constants obtained for the first row TM dimers while Section V describes the same information for the second row TM dimers and discusses some of the differences between the first and second row TM dimers. Section VI discusses the electron correlation problem for Cr_2 and discusses some possible future approaches that might be used. These future approaches are discussed in relation to some of the current more approximate techniques. Finally Section VII presents the conclusions from this work.

II. Qualitative Features of the Bonding in the TM Dimers

We first consider some features of the TM atoms, in particular the relative (n+1)s and nd orbital sizes, the nd-nd exchange terms, and the ordering and separations of the low-lying atomic states[15]. These properties of the atoms are important because they control the atomic states available for bonding, the strength of the nd-nd bonds and the nature of the bonding i.e. whether the bonding orbitals involve predominately (n+1)s or nd character. Table I shows the following properties i)$\langle r_{(n+1)s}\rangle/\langle r_{nd}\rangle$, obtained form numerical Hartree-Fock calculations for the $(n+1)s^1nd^{m+1}$ state ii) the $(n+1)s^2nd^m \rightarrow (n+1)s^1nd^{m+1}$ excitation energy and iii) the $(n+1)s^2nd^m \rightarrow nd^{m+2}$ excitation energy. Looking first at the relative orbital sizes we see that for the first transition row the ratio $\langle r_{4s}\rangle/\langle r_{3d}\rangle$ increases monotonically from 2.03 for Sc to 3.36 for Cu. The same trend is seen for the second transition row but here the 5s and 4d orbital sizes are more comparable. The increase in $\langle r_{(n+1)s}\rangle/\langle r_{nd}\rangle$ as one moves

across a row is due to increased shielding of the nuclear charge by the nd electrons.

Looking next at the excitation energies, the ground state for the first few elements of the first and second transition rows is the $(n+1)s^2nd^m$ state. The trends in the $(n+1)s^2nd^m \rightarrow (n+1)s^1nd^{m+1}$ excitation energies depend on two competing factors i) the stabilization of the nd level with respect to the (n+1)s level as the nuclear charge increases and ii) the number of nd-nd exchange terms. Up to the point that the nd shell is half filled both of these factors favor the $(n+1)s^1nd^{m+1}$ state for larger nuclear charge since movement of an s electron into the d shell increases the number of nd-nd exchange terms. This leads to a monotonic decrease in the excitation energies from Sc to Cr and from Y to Mo. Starting with Mn or Tc, the excited state has one more doubly occupied nd orbital in each case than the ground state. Thus, s to d promotion leads to loss of nd-nd exchange terms and a strong preference for the $(n+1)s^2nd^5$ state resulting in a discontinuity between Cr-Mn and Mo-Tc. However, from Mn to Cu and Tc to Ag, there is once again a monotonic decrease in the excitation energy due to the stabilization of nd with respect to (n+1)s for increasing nuclear charge. From Table I one also sees that the nd^{m+2} state is an excited state for the first transition row but becomes a low-lying state for the right half of the second transition row. In fact $4d^{10}$ is the ground state configuration for Pd.

For the molecules considered here the atomic states which are sufficiently low-lying to be available for bonding are the $(n+1)s^2nd^m$ and $(n+1)s^1nd^{m+1}$ states. These two states lead to three different atomic asymptotes: i) $(n+1)s^2nd^m + (n+1)s^2nd^m$, ii) $(n+1)s^2nd^m + (n+1)s^1nd^{m+1}$ and iii)

$(n+1)s^1nd^{m+1} + (n+1)s^1nd^{m+1}$. The accessibility of these asymptotes of course depends on the $(n+1)s^2nd^m \rightarrow (n+1)s^1nd^{m+1}$ excitation energy. Thus for the first transition row we find that for Sc_2 the low-lying states arise from the first two asymptotes with $4s^13d^{m+1} + 4s^13d^{m+1}$ too high in energy to lead to the ground state, while for Ti_2, V_2, Cr_2, and Cu_2 the ground states arise from the $4s^13d^{m+1} + 4s^13d^{m+1}$ atomic asymptote.

For the first transition row, because the 4s orbital is significantly larger than the 3d orbital the predominant interaction in the TM dimers at large internuclear separation (R) is between the 4s orbitals with very little 3d interaction. For states arising from the $4s^23d^m + 4s^23d^m$ atomic asymptote this interaction is basically repulsive and only a shallow well at large R_e (approximately. 8.0 a_0) arising from the $4s \rightarrow 4p$ near degeneracy effect is observed. For states arising from the $4s^23d^m + 4s^13d^{m+1}$ atomic asymptote the 4s interaction is weakly bonding at intermediate R but is repulsive at small R leading to intermediate R_e values(approximately 5.0 a_0). At these R_e values the 3d-3d overlaps(S) are small which favors one-electron 3d bonds, (ie. one electron per bonding orbital as in H_2^+, a bond order of one half) whose bonding terms vary with distance like S, over two-electron 3d bonds (ie. two electrons per bonding orbital as in H_2, a bond order of one), whose bonding terms vary with distance like S^2[17]. Finally for states arising from the $4s^13d^{m+1} + 4s^13d^{m+1}$ atomic asymptote the 4s-4s portion of the interaction is attractive and also appears to not become repulsive until well inside the optimal 4s-4s bonding radius. Thus, states arising from this atomic asymptote favor short R_e regions where the 3d-3d overlaps are large enough to permit two-electron 3d bonding.

The strength of multiple one-electron nd bonds is determined mainly

by overlap considerations, since the resulting singly occupied orbitals are orthogonal and high spin coupled, leading to no loss of atomic exchange interactions. The relative overlaps of nd orbitals are nd$\sigma \approx$nd$\pi >$ndδ. Thus, the ndσ and ndπ orbitals are filled first. An example of such bonding is the $^5\Sigma_u^-$ state of Sc_2, which has three one-electron 3d bonds of σ and π symmetry.

The strength of multiple two-electron nd bonds is determined both by the overlap of the orbitals and by the size of the atomic exchange terms which are lost due to bond formation. Overlap considerations primarily determine the occupation of the bonding orbitals. Since two electron bonds vary with R as S^2, and one-electron bonds as S, the ndδ bonding is even less favorable relative to ndσ and ndπ than for one-electron bonds. Thus, for Ti_2 the $^1\Sigma_g^+$ state which arises from $4s^13d^3 + 4s^13d^3$ has three two-electron 3d bonds with bonding orbitals of σ and π symmetry. It is interesting that in the region where the ndσ and ndπ orbitals have large overlaps leading to two-electron bonds, the overlaps of the ndδ orbitals are so small that one-electron bonds are favored. For example in going from Ti_2 to V_2 the two electrons which are added to the 3dδ preferentially couple high spin leading to a $^3\Sigma_g^-$ ground state. When two additional electrons are added into the 3dδ orbital as in the ground $^1\Sigma_g^+$ state of Cr_2, the overall bonding becomes much weaker. This shows that doubly occupying the 3dδ orbitals is unfavorable; although part of the difference between V_2 and Cr_2 involves 3d-3d exchange interactions.

One measure of the atomic exchange interaction is the relative energies of the atomic states as the coupling of the nd electrons is changed (we use Moore[16] to estimate the importance of this effect). For Sc, $4s^13d^2$,

the energy needed to change the 3d coupling from ^3F in the ^4F state to ^1D in the ^2D state is 0.8eV. For Ti $4s^13d^3$, $4s^13d^3(^2G)$ ^3G is 1.0eV above $4s^13d^3(^4F)$ ^5F. By Cr, with the maximum open 3d orbitals, this value has reached 2.5eV. This means that the 3d-3d bonds are expected to be weaker for Cr_2 unless the bond length shortens to increase the 3d-3d overlap.

For the TM elements with more than half filled 3d shells, the formation of 3d bonds becomes much less favorable for two reasons. First the ratio of 4s to 3d orbital sizes is larger for the right half of the first transition row. Secondly the presence of doubly occupied 3d orbitals leads to repulsive interactions which effectively cancel any bonding interactions from the 3d shell. Thus the bonding here is dominated by the 4s electrons.

For the second transition row the qualitative features of the bonding from the corresponding three atomic asymptotes are similar. However, the more comparable 5s and 4d orbital sizes as well as the smaller 4d exchange terms lead to stronger 4d bonding. Hence the $4d\delta$ overlaps appear to be more comparable to the $4d\sigma$ and $4d\pi$ overlaps as evidenced by a low-lying state of Nb_2 with occupation $4d\sigma_g^1 4d\pi_u^4 4d\delta_g^3$. Also for the right hand side of the second transition row the $4d^{m+2}$ atomic states are available for bonding. An additional important difference is that relativistic effects become quite important for the right half of the second transition row (see Ref. 18, for example). It is for this reason that the current all-electron studies are restricted to the lighter elements of the second transition row.

III. Calculational Details

As noted in the previous section, both the $(n+1)s^2nd^m$ and $(n+1)s^1nd^{m+1}$ states of the atoms are important in the bonding in the dimers. Hay [19] was one of the first to realize that the basis sets optimized for the $(n+1)s^2nd^m$

states yield a very poor description of the $(n+1)s^1nd^{m+1}$ states, but by optimizing one additional d function for the $(n+1)s^1nd^{m+1}$ occupation, the separation between the $(n+1)s^2nd^m$ and $(n+1)s^1nd^{m+1}$ occupations was very close to that obtained in numerical Hartree-Fock calculations. When (n+1)s bonding is present, due to the near degeneracy of the (n+1)s and (n+1)p orbitals, the basis set requires p functions in the same region. Since the (n+1)p orbital is not occupied, such functions are missing in the atomic basis sets. One common approach is to optimize two additional p functions for the $(n+1)s^1(n+1)p^1nd^m$ occupation and then multiply the exponents of the additional functions by from 1.2 to 1.5 to bring them more into the region of the (n+1)s function [20]. The final concern in the basis set is f functions to help describe any d-d bonds. For Cu_2 with a 4s-4s bond or Sc_2 with one-electron d bonds, the addition of f polarization functions has very little effect. However, McLean and Liu [21] have shown that for Cr_2, with two-electron d bonding, the addition of f functions lowers the energy by more than 1eV at the SCF level. Thus it is important to have f functions, especially when comparing one state which has one-electron nd bonds with another that has two-electron nd bonds, such as in Ti_2.

The basis sets used in this work meet these requirements. For the first row transition elements the basis set is a (14s11p6d3f)/ [8s6p4d2f] segmented contraction based on Wachters' basis set[20] plus his 4p(multiplied by 1.5) and the Hay diffuse 3d[19]. The 4f functions are optimized at the CI level for the $4s^13d^{m+1}$ state of the atom (note that for the Cu_2 calculations the three f functions were contracted to one). For the second transition row elements the basis set is a (17s13p9d2f)/[6s5p5d1f] general contraction

based on Huzinaga's basis set[22] plus 5p(multiplied by 1.3), diffuse 4d, and 4f functions as optimized by Walch, Bauschlicher, and Nelin[23]. The 3s function arising from the d, as well as the 4p functions arising from the f functions were removed.

In this work we use the CASSCF approach to perform the MCSCF calculations. Ideally one would like to include the nd, (n+1)s and (n+1)p orbitals in the active space to allow the formation of both the s-s bond and nd-nd bonds and to account for the (n+1)s to (n+1)p near degeneracy. More extensive correlation could then be included with a CI calculation. However, even the CASSCF treatment is not always possible. The first approximation we make is to remove the (n+1)p orbital from the active space, except for Sc_2 and Y_2 which arise from the $(n+1)s^2nd^m$ + $(n+1)s^1nd^{m+1}$ atomic limit. Here the (n+1)p orbital should be included in the active space since the (n+1)s to (n+1)p near degeneracy is important for the $(n+1)s^2nd^m$ state of the atom. For the remaining systems which arise from the $(n+1)s^1nd^{m+1}$ + $(n+1)s^1nd^{m+1}$ atomic limit the (n+1)p does not contribute for the atom and tests show that omitting the (n+1)p leads to less binding energy at the CASSCF level(due to angular correlation effects which vanish at large R), but virtually the same D_e when correlation is added. Thus, this approximation effects only those calculations for which only CASSCF calculations were performed.

The second approximation is to restrict the number of active electrons in σ, π and δ symmetry. The constraints are similar in spirit to those in the GVB wavefunction[5]. As an example of the GVB wavefunction consider the $^1\Sigma_g^+$ state of Ti_2 which has the configuration

$4s\sigma_g^2\ 3d\sigma_g^2\ 3d\pi_{x_u}^2\ 3d\pi_{y_u}^2$

ie. a quadruple bond with $4s\sigma$, $3d\sigma$, and $3d\pi$ bonds. The configurations in the GVB wavefunction consist of a geminal product of the three possible configurations constructed from the bonding and antibonding orbitals of each pair ie. 81 configurations in the case of four pairs. This wavefunction dissociates to neutral atoms and also allows spin recoupling. In the CASSCF calculations it is not possible to do precisely the GVB calculation since the configuration space must be a product of full CI calculations within each symmetry type. Consistent with these constraints we restrict four electrons to the four σ orbitals, two electrons to the two π_x orbitals, and two electrons to the two π_y orbitals. The δ orbitals would not be active in this calculation since they are forced to have no electrons by our constraints. For the other cases the constraints are not specifically stated but can be inferred from the principle configuration given.

The last approximation which was made only for the second transition row dimers is to freeze the deep core orbitals, the n=1,2,3 shells and 4s orbitals at their atomic forms, based on a high spin SCF calculation at R=50.0 a_0, while the 4p and valence (5s, 5p, and 4d) orbitals are optimized at each distance. Since the core orbitals are expected to be atomic like, this approximation will have negligible effect on the results, but results in some computational savings.

When it is possible, we follow the CASSCF calculations with multi-reference singles and doubles CI calculations. In these calculations only the electrons arising from the (n+1)s and nd shells of the atom are correlated. The references configurations are selected as the most important configurations in the CASSCF wavefunction. In general the most important configurations are found to be the leading terms in the GVB geminal ex-

pansion. Different reference lists were used near R_e and at long range. The long distance points were computed using the high spin SCF wavefunction as the reference configuration, while the points near R_e use the CASSCF wavefunction.

The calculations for the first transition row dimers use the MOLECULE [24]-SWEDEN[25] programs while the calculations for the second transition row dimers use BIGGMOLI[26]-SWEDEN.

IV. First Row Transition Metal Dimers

Fig.1 shows calculated potential curves for low-lying states of Sc_2 while Table II shows calculated spectroscopic constants for all the first row TM dimers. The dominant configurations for the states considered here are:

$^5\Sigma_u^-$ $4s\sigma_g^2$ $3d\sigma_g^1$ $4s\sigma_u^1$ $3d\pi_{xu}^1$ $3d\pi_{yu}^1$

$^3\Sigma_g^-$ $4s\sigma_g^2$ $4s\sigma_u^2$ $3d\pi_{xu}^1$ $3d\pi_{yu}^1$

$^1\Sigma_g^+$ $4s\sigma_g^2$ $4s\sigma_u^2$ $3d\sigma_g^2$

$^3\Sigma_u^+$ $4s\sigma_g^2$ $4s\sigma_u^2$ $3d\sigma_g^1$ $3d\sigma_u^1$

The initial study of Sc_2 by Walch and Bauschlicher[17] found only weakly bound states arising out of the $4s^23d^1 + 4s^23d^1$ asymptote in contrast to mass spectrometric experiments[27] which indicated strong bonding ($De=1.1\pm0.2eV$). A $^5\Sigma_u^-$ state was found which was bound by about 0.8 eV with respect to the $4s^23d^1 + 4s^14p^13d^1$ atomic limit, but unbound with respect to $4s^23d^1 + 4s^23d^1$. However at about the same time that this work was published, matrix isolation studies by Knight, VanZee, and Weltner[28] indicated a bound $^5\Sigma$ state of Sc_2. From ESR studies it appeared that this state arose from the $4s^23d^1 + 4s^13d^2$ atomic asymptote which had not been studied in detail in the previous theoretical studies.A reexamination of this system[30] revealed a new $^5\Sigma_u^-$ state which had been missed in the previous study because its R_e(about 5.0 a_0) is much shorter than the R_e values for the states studied previously (about 7.0 a_0). The $^5\Sigma_u^-$ state turned out to be of considerable theoretical interest because it exhibited multiple 3d bonding(three one-electron bonds) and constituted the first theoretical evidence of multiple 3d bonding in a first row transition metal dimer. The D_e given in Table II is obtained from the CI calculations by computing the binding energy of the $^5\Sigma_u^-$ state with respect to the $4s^23d^1 + 4s^13d^2$

asymptote and then subtracting the experimental asymptotic separation to give the D_e with respect to $4s^23d^1 + 4s^23d^1$. The resulting D_e of 0.44 eV and ω_e of 184 cm^{-1} are in reasonable accord with experimental values of D_e=1.1eV[27] and ω_e=238.9 cm^{-1}[29].

Adding two electrons to the 3dδ orbitals of the $^5\Sigma_u^-$ state of Sc_2 and high spin coupling the 3d electrons leads to the $^7\Sigma_u^+$ state of Ti_2. The Ti_2 $^7\Sigma_u^+$ state, like the Sc_2 $^5\Sigma_u^-$ state comes from the $4s^23d^m + 4s^13d^{m+1}$ asymptote. These states have long bond lengths(R_e greater than 5.0 a_0) and small vibrational frequencies(ω_e about 200 cm^{-1}) The states of Ti_2 which are considered here have the configurations:

$^7\Sigma_u^+$ $4s\sigma_g^2$ $3d\sigma_g^1$ $4s\sigma_u^1$ $3d\pi_{xu}^1$ $3d\pi_{yu}^1$ $3d\delta_{xyg}^1$ $3d\delta_{(x^2-y^2)g}^1$

$^1\Sigma_g^+$ $4s\sigma_g^2$ $3d\sigma_g^2$ $3d\pi_{xu}^2$ $3d\pi_{yu}^2$

For Ti_2 in Table I one sees that the excitation energy to the $4s^13d^{m+1}$ $+4s^13d^{m+1}$ atomic asymptote is about half as large as for Sc_2. Thus the $^1\Sigma_g^+$ state which arises from the $4s^13d^3 + 4s^13d^3$ atomic asymptote becomes a competitor for the ground state of Ti_2. The bonding here is a triple two electron 3d bond(3dσ, 3dπ_x, and 3dπ_y). This leads to a short R state, R_e=3.72 a_0 and ω_e=438cm^{-1}. The bond length here is not known experimentally but the experimental vibrational frequency is 407.9 cm^{-1}[29] which is consistent with the $^1\Sigma_g^+$ state of Ti_2, but inconsistent with the $^7\Sigma_u^+$ state. Based on this we tentatively assign the ground state of Ti_2 as $^1\Sigma_g^+$ although the calculations place $^1\Sigma_g^+$ 0.40 eV above $^7\Sigma_u^+$.

Table II also shows the calculated D_e of Ti_2. Here we see that CASSCF obtains only a small percentage of the binding energy. The CI wavefunction consists of a MRSDCI from nine references (more than 180,000 CSFs). The calculated binding energy here is 1.94 eV compared to an experimental

D_e of 2.91 eV [31] (all referenced to $4s^13d^3 + 4s^13d^3$). Thus even when more extensive correlation is added, the order of the states is not changed. However, CI calculations describe high spin states better than low spin states; the $^1\Sigma_g^+$ is not as well described as $^7\Sigma_u^+$. Considering the difficulty in describing multiple two-electron 3d bonds, as measured by the errors in D_e, it would not be surprising to find that a better calculation would reverse the order of the states. Thus trends in the correlation treatments also support the $^1\Sigma_g^+$ assignment of the ground state.

Fig. 2 shows calculated potential curves for the $^3\Sigma_g^-$, and $^1\Gamma_g$ states of V_2. The dominant configurations for the states considered here are:

$^3\Sigma_g^-$ $4s\sigma_g^2\ 3d\sigma_g^2\ 3d\pi_{xu}^2\ 3d\pi_{yu}^2\ 3d\delta_{xyg}^1\ 3d\delta_{(x^2-y^2)g}^1$

$^3\Delta_g$ $4s\sigma_g^2\ 3d\sigma_g^1\ 3d\pi_{xu}^2\ 3d\pi_{yu}^2\ 3d\delta_{xyg}^2\ 3d\delta_{(x^2-y^2)g}^1$

The $^3\Sigma_g^-$ state of V_2 has the same triple two-electron 3d bond as in Ti_2 with the remaining two electrons in the $3d\delta$ orbitals. Because the $3d\delta$ orbitals still have small overlaps in the region near R_e(about 3.5 a_0), the lowest state is a triplet state arising by forming two one-electron $3d\delta$ bonds. This occupation also gives rise to $^1\Gamma_g$ and $^1\Sigma_g^+$ states analogous to the corresponding states of the $\pi_u^4\pi_g^2$ occupation of O_2. The R_e and ω_e values obtained from the CASSCF curves[9] are in good agreement with the recent results of Langridge-Smith, Morse, Hansen, Smalley, and Merer[32] for the $^3\Sigma_g^-$ ground state of V_2. The presence of a very low-lying state (possibly $^1\Sigma_g^+$) was indicated by the spectral analysis of Merer[33] and is consistent with the very low-lying $^1\Gamma_g$ state($^1\Sigma_g^+$ is obtained as a second root of the CASSCF and is also very low-lying). Table II also shows the calculated spectroscopic constants for the $^3\Delta_g$ state of V_2. This state was studied because the corresponding state is very low-lying for Nb_2 but here

the excitation energy $^3\Sigma_g^- \rightarrow {}^3\Delta_g$ is 0.92 eV.

Fig.3 shows calculated potential curves for Cr_2. Here the 3dδ orbitals are doubly occupied which is expected to be unfavorable based on the V_2 result that the 3dδ orbitals were preferentially singly occupied. This is consistent with the weaker bonding in Cr_2, D_e=1.6eV[34] as compared to V_2, D_e=3.0eV[31].Because of the weaker bonding in Cr_2 the CASSCF potential curve is not bound[9].However the potential curve does exhibit a shoulder near the experimental R_e which is suggestive of an inner well. As discussed in section VI a more accurate computational description of the quintuple 3d bond in Cr_2 is a very difficult problem which remains as a major challenge for theory.

Fig. 4 shows calculated potential curves for TiV while Table III summarizes the calculated spectroscopic constants. The $^4\Sigma^-$, $^4\Pi$, and $^2\Delta$ states may be derived from the V_2 $^3\Sigma_g^-$ configuration by removing a single electron from the 3dσ, 3dπ, and 3dδ orbitals, respectively. The ordering of these states may be understood on the basis of orbital overlap and intra atomic coupling[35] arguments. Based on atomic overlap arguments one expects the ordering

$$^2\Delta < {}^4\Sigma^- < {}^4\Pi$$

However, while all these states dissociate to pure V ^{6}D and the $^4\Sigma^-$ and $^4\Pi$ states dissociate to pure Ti ^{5}F, the $^2\Delta$ state dissociates to a mixture of 20 % Ti ^{5}F and 80 % Ti ^{5}P. It is this latter intra atomic coupling effect which leads to the observed ordering of states with

$$^4\Sigma^- < {}^2\Delta < {}^4\Pi$$

The calculated $^4\Sigma^-$ ground state is consistent with the experimental results of Van Zee and Weltner which show an ESR spectrum consistent

with $^4\Sigma^-$[36]. The calculated bond length of TiV is intermediate between the bond lengths of Ti_2 and V_2.

Table II also shows results for the $^1\Sigma_g^+$ state of Cu_2. The electronic configuration here is:

$$^1\Sigma_g^+ \; 4s\sigma_g^2 \; 3d\sigma_g^2 \; 3d\sigma_u^2 \; 3d\pi_u^4 \; 3d\pi_g^4 \; 3d\delta_u^4 \; 3d\delta_g^4$$

This configuration arises from the $4s^13d^{10} + 4s^13d^{10}$ asymptote. The bonding here appears to involve mainly the 4s electrons with the 3d electrons remaining essentially atomic like[37], [38]. However, this viewpoint has been challenged by Pauling who argues in favor of $4s^14p^13d^9$ hybrids[39]. A central concern for the Cu_2 calculations has been the calculation of the bond length. Here we find that correlation of the 3d electrons shortens the bond by 0.19 a_0 leading to a final bond length of 4.35 a_0 which is 0.15 a_0 longer than experiment. It has been argued[37] that the remaining discrepancy is largely due to relativistic effects since twice the relativistic contraction of the 4s orbital for the $4s^13d^{10}$ state is 0.13 a_0. Since that time calculations have shown that only about 70% of the atomic core-valence contraction in the alkali dimers is observed in the molecular systems[40]. Martin[41] using an all electron treatment which includes relativistic effects as a perturbation and Laskowski et.al.[42] who have added relativistic effects through an effective core potential approach, both compute the contraction to be 0.10 a_o, or about 70% of the atomic contraction. In both approaches[41,42] correlation does not effect this conclusion. More recently Martin and Werner[43] have considered the effect of higher excitations with CEPA, in addition to the relativistic effects, and find a bond length in good agreement with experiment. It has been observed[44] that a POLCI treatment leads to a better D_e for Cu_2 than a SDCI treatment. However, it is not

clear that such approximations can be used for those systems where there is d-d bonding.

V. Second Row Transition Metal Dimers

Fig. 5 shows calculated potential curves for selected states of Y_2. The dominant configurations for the states considered here are:

$^1\Sigma_g^+$ $5s\sigma_g^2$ $4d\pi_{xu}^2$ $4d\pi_{yu}^2$

$^5\Sigma_u^-$ $5s\sigma_g^2$ $5s\sigma_u^1$ $4d\sigma_g^1$ $4d\pi_{xu}^1$ $4d\pi_{yu}^1$

$^1\Delta_g$ $5s\sigma_g^2$ $5s\sigma_u^2$ ($4d\pi_{xu}^2$ - $4d\pi_{yu}^2$)

$^1\Sigma_g^+$ $5s\sigma_g^2$ $5s\sigma_u^2$ $4d\sigma_g^2$

The $^5\Sigma_u^-$ state here is directly related to the $^5\Sigma_u^-$ state of Sc_2 and arises from the $5s^24d^1 + 5s^14d^2$ atomic asymptote. The long R $^1\Sigma_g^+$ and $^1\Delta_g$ states arise from the $5s^24d^1 + 5s^24d^1$ asymptote. The long R $^1\Sigma_g^+$ state is directly related to the Sc_2 $^1\Sigma_g^+$ state, while the $^1\Delta_g$ state was not studied for Sc_2 but arises from the same configuration (π_u^2) as the $^3\Sigma_g^-$ state of Sc_2. A new state for Y_2 which was high in energy for Sc_2 is the short R $^1\Sigma_g^+$ state which arises from the $5s^14d^2 + 5s^14d^2$ atomic asymptote. That this state is low-lying for Y_2 but not for Sc_2 reflects the significantly greater 4d bonding in the second transition row. An unusual feature of the short R $^1\Sigma_g^+$ potential curve is an apparent avoided crossing; the state which is crossing the short R $^1\Sigma_g^+$ state is a $^1\Sigma_g^+$ state derived from the same configuration as the $^1\Delta_g$ state. This $^1\Sigma_g^+$ state should lie slightly above the $^1\Delta_g$ curve. An interesting feature of the Y_2 potential curves as compared to the Sc_2 potential curves is the more comparable R_e values for states arising out of the three possible asymptotes. This result is consistent with the more comparable (n+1)s and nd orbital sizes for the second transition row as compared to the first transition row. Table IV gives calculated spectroscopic constants for the second transition row dimers. No experimental data exist for Y_2. However, Weltner does not observe an ESR

spectrum for Y_2 as was observed for Sc_2[45]. One possible explanation for this is that the $^1\Sigma_g^+$ state is actually the ground state for Y_2 even though the calculations place it 0.87 eV above the $^5\Sigma_u^-$ state;here as discussed above for Ti_2 we expect more extensive CI calculations to favor the $^1\Sigma_g^+$ state over the $^5\Sigma_u^-$ state. As was done for the first transition row the T_e values are obtained by computing the binding energy for each state with respect to its corresponding asymptote and then positioning the asymptotes at the experimental separations. Thus we are including a correction for the error in the Y_2 asymptotic energies due to relativistic effects. Further experiments would be necessary to decide definitely whether $^1\Sigma_g^+$ is the ground state of Y_2. Here the most useful experimental result would be a measurement of R_e since R_e differs significantly between the short R $^1\Sigma_g^+$ and the $^5\Sigma_u^-$ state whereas the vibrational frequencies are not substantially different.

Fig. 6 shows calculated potential curves for Nb_2 while the calculated spectroscopic constants are given in Table IV. The dominant configurations for the states considered here are:

$^3\Sigma_g^-$ $5s\sigma_g^2\ 4d\sigma_g^2\ 4d\pi_{xu}^2\ 4d\pi_{yu}^2\ 4d\delta_{xyg}^1\ 4d\delta_{(x^2-y^2)g}^1$

$^3\Delta_g$ $5s\sigma_g^2\ 4d\sigma_g^1\ 4d\pi_{xu}^2\ 4d\pi_{yu}^2\ 4d\delta_{xyg}^2\ 4d\delta_{(x^2-y^2)g}^1$

$^3\Phi_g$ $5s\sigma_g^2\ 4d\sigma_g^2\ 4d\pi_u^3\ 4d\delta_g^3$

Here the $^3\Sigma_g^-$, $^1\Gamma_g$, $^1\Sigma_g^+$, and $^3\Delta_g$ states are directly related to the corresponding states of V_2. The $^3\Delta_g$ and $^3\Phi_g$ states arise by exciting an electron from $4d\sigma$ and $4d\pi$, respectively, into $4d\delta$. From Fig. 6 one sees that the electronic structure of Nb_2 seems very similar to that of V_2 in that the lowest calculated state is $^3\Sigma_g^-$ and there is a low-lying $^1\Gamma_g$ state. There are, however, two additional low-lying states $^3\Delta_g$ and $^3\Phi_g$. Here the

$^3\Delta_g$ state is very close in energy to the $^3\Sigma_g^-$ state while the $^3\Phi_g$ state is 0.96eV higher. The ordering of these states is consistent with the ordering of the $^4\Sigma^-$ and $^4\Pi$ states of TiV. The increased stability of $^3\Delta_g$ for Nb_2 as compared to V_2 implies stronger 4dδ bonding in Nb_2 as compared to the 3dδ bonding in V_2. This is also consistent with the stronger bonding observed in Nb_2 (calculated D_e=2.24 eV) as compared to V_2(calculated D_e=0.60 eV).

Experimentally very little is known about the electronic structure of Nb_2. Smalley has obtained the optical spectrum of Nb_2 but the spectrum shows little resolved structure and is too complex to enable analysis[46]. The calculations also show this increased complexity in the Nb_2 spectrum due to the presence of a low-lying $^3\Delta_g$ state in addition to the $^1\Gamma_g$ and $^1\Sigma_g^+$ states which were also present for V_2. Also for Nb relativistic effects are much larger than for V and may increase the coupling of states. As for Y_2 some experimental information would be very useful here especially a determination of R_e which could help to distinguish between the $^3\Delta_g$ and $^3\Sigma_g^-$ states as candidates for the ground state of Nb_2.

In order to compare Cr_2 and Mo_2 the ground $^1\Sigma_g^+$ state of Mo_2 was considered at the CASSCF level. This state has the configuration

$$^1\Sigma_g^+ \; 5s\sigma_g^2 \; 4d\sigma_g^2 \; 4d\pi_{xu}^2 \; 4d\pi_{yu}^2 \; 4d\delta_{xy,g}^2 \; 4d\delta_{(x^2-y^2)g}^2$$

which is directly related to the ground state configuration of Cr_2. Mo_2 differs from Cr_2 in that the CASSCF curve is bound due to increased nd bonding for the second transition row. The calculated spectroscopic constants here are(experimental values [47,48] in parenthesis) R_e=1.99A(1.93A), ω_e=399cm^{-1}(477cm^{-1}) and D_e= 0.77eV(4.2$\pm$0.2eV).

VI. The Description of Electron Correlation in Cr_2

As indicated in section IV Cr_2 might be viewed as a failure of the CASSCF procedure since only a shoulder is obtained in the region where one expects an inner well(3d bonding region). However, the CASSCF procedure with this choice of active space is only a first order description of Cr_2 which allows the spin recoupling of the 4s and 3d electrons from the large R high spin atomic coupling to the region near R_e where the system can be described formally as a hextuple bond, but does not include all of the molecular correlation effects. The particular features of Cr_2 which make the description of the region near R_e so difficult are i)that we are dealing with a quintuple bond and ii) that the 3d overlaps are smaller even near R_e than would be the case for say 2p orbitals in a first row molecule. The result is that Cr_2 is a molecule which requires a complex MCSCF zero order description involving very high orders of excitation with respect to a single configuration SCF reference.

In order to quantify this somewhat we carried out small valence CI calculations among the active orbitals from the CASSCF calculation(for $R=3.25a_0$). Here we allowed single and double excitations from various subsets of the most important configurations in the CASSCF wavefunction. The first calculation which used as reference configurations the 16 configurations which are doubles or less from SCF and thus included up to quadruples with respect to SCF led to a valence energy 2.42 eV above the CASSCF energy. We then added all the quadruples which are important in the CASSCF(16 more configurations) so that we are including through hextuples and obtained an energy 0.70 eV above the CASSCF energy. Finally we added the hextuple excitations(6 more configurations) which are important in the CASSCF so that we are now including through octuple excita-

tions and the resulting energy was still 0.42 eV above the CASSCF energy. From analysis of the configurations which need to be included to get a reasonable valence energy we see that the reference configurations must include quadruple excitations among the 3dδ orbitals and double excitations among the 3dσ and 3dπ orbitals but that the 4s bonding orbital may remain inactive(i.e. doubly occupied in all reference configurations). This result is in line with the relative overlaps of these orbitals and suggests that the 3dδ orbitals are still in the small overlap region even near R_e. One also expects that V_2 would be easier to describe than Cr_2 since the 3dδ orbitals are singly occupied.

The CASSCF procedure used does not include all of the important molecular correlation effects. For the TM atoms the most important additional correlation effects are derived from the 4p, 3d$'$(here 3d$'$ is a tight diffuse correlating orbital for the 3d) and 4f orbitals and we expect the most important additional molecular correlation terms to involve these orbitals. One approach to introducing these missing correlation effects would be the direct use of multi configuration singles and doubles CI. However, if we use the CASSCF wavefunction(3088 configurations) as a reference the CI expansion is 57 million configurations for a [8s6p4d2f] basis set. However, given the difficulty in reproducing the CASSCF energy for smaller numbers of reference configurations it is clear that any CI calculation with fewer references than the CASSCF wavefunction will have to be carried out with caution.

Given these difficulties several alternative methods have been tried for introducing the missing molecular correlation in approximate ways. By far the most extensive study of additional correlation effects and additivity of

correlation effects for Cr_2 is that of Walch[12]. In the extended CASSCF calculations of Walch, the 3d′ shell and 4p shell are added to the CASSCF calculation. This approach would be rigorous if one could include all the additional active orbitals in one calculation. Unfortunately, this is not possible even with orbital occupation constraints and a procedure was used in which the extra active orbitals were added by symmetry block and the separately obtained energy contributions were summed to obtain an estimate of the extra molecular correlation. The problem with the method is that it assumes that the atomic correlation is constant with R, however, "atomic correlation" is reduced as the bonds form. For Ti_2 calculations can be carried out in which all the 3d′ orbitals are included simultaneously and it is found that the extended CASSCF procedure overestimates the effect of 3d′ by a factor of four due mostly to the variation with R of the 3d′ atomic correlation terms. On the other hand comparisons of extended CASSCF calculations and CI calculations for N_2 and Ti_2 indicate that the approach of summing the individual contributions does not give a potential curve that is deeper than the CI curve and that the overestimation of the effect of 3d′ does not effect the R_e or ω_e significantly. Thus, we conclude that the reasonable potential curve obtained for Cr_2 by Walch (see Fig. 3) must arise at least in part by cancellation of errors ie. the overestimation of the effect of 3d′ is being compensated for by the omission of other molecular correlation effects such as correlation involving 4f. The calculated spectroscopic constants are (experimental values[34,49-51] in parenthesis) R_e=1.78A(1.68A), ω_e =383cm^{-1}(480cm^{-1}), and D_e=0.71eV(1.56eV). These results, while in part due to cancellation of errors, do indicate the importance of 3d′ and 4p for more extensive CI calculations.

Another approach due to Das and Jaffe[13], is in principle equivalent to the extended CASSCF approach used by Walch. These workers use symmetrically orthogonalized atomic orbitals (called PLO's) in an attempt to greatly reduce the size of the MCSCF expansion. Thus, Das and Jaffe did not attempt to reproduce the valence correlation in the CASSCF calculations[9], but rather computed additional correlation effects and then added them to our CASSCF potential curve. They predict that 3d′ and also 3p shell excitations contribute to the binding energy. Due to limitations in the CI expansion and the small basis used, their conclusions while interesting are somewhat tentative.

A computationally very different approach due to Goodgame and Goddard[14] assumes that the missing correlation serves mainly to correct the location of the ionic atomic asymptotes. Those authors attempt to include these effects by empirical modification of the integrals to correct the atomic ionization potentials and electron affinities to agree with experiment This method does lead to a reasonable potential curve for Cr_2 although the bond length is somewhat too short which suggests that this method over corrects to some extent.

The main value of these approximate approaches is expected to be to lead to a better understanding of the additional correlation effects needed to compute a reliable potential curve for Cr_2. In the opinion of the present authors the most promising theoretical method for actually doing the large CI calculations necessary to solve the Cr_2 problem is the externally contracted CI method[52]. These calculations will still be difficult due to the need for an extensive reference wavefunction leading to a few million configurations. However, it is probable that these calculations will be

carried out within the next few years.

VII. Conclusions.

The CASSCF procedure is found to generally provide reliable R_e and ω_e values. However, D_e values are systematically underestimated at the CASSCF level; the worst case is Cr_2 where the CASSCF curve is not bound although a shoulder is observed in the region near the experimental R_e. The CASSCF procedure provides a consistent set of calculations for these molecules from which qualitative trends and a picture of the electronic structure may be derived.

The CASSCF/CI procedure has lead to confirmation of the $^5\Sigma_u^-$ ground state of Sc_2 and the $^4\Sigma^-$ ground state of TiV. Numerous predictions remain untested. Among these are the prediction that Ti_2 has a $^1\Sigma_g^+$ ground state with a short bond length and essentially all the computed results for Y_2 and Nb_2. The computed results for Nb_2 are especially interesting since the experimental spectrum for Nb_2 is so complex that it has not been analyzed. Experiment has confirmed the prediction of the ground state symmetry and bond length of V_2.

In addition to specific predictions, these studies yield a simple qualitative picture of the bonding in the transition metal dimers. The $4s^23d^m + 4s^23d^m$ asymptote leads to Van der Waals bonding at large R due to the $4s \rightarrow 4p$ near degeneracy effect. Here the 3d electrons are only weakly coupled. These weakly bound states have not been observed in experiment, and probably are not of chemical interest. If the two atoms have the occupation $4s^13d^{m+1}$ strong two-electron d-d bonds (ie. two electrons per bond orbital as in H_2, a bond order of one) and a short bond length results. Such bonding has been observed for Ti_2 $^1\Sigma_g^+$, V_2 $^3\Sigma_g^-$, and Cr_2 $^1\Sigma_g^+$.

When the excitation energy is very large the cost of promoting both atoms to the occupation $4s^1 3d^{m+1}$ is so large that bonding arises from the mixed asymptote; $4s^1 3d^{m+1} + 4s^2 3d^m$. Such bonding has been found for Sc_2 $^5\Sigma_u^-$ and Ti_2 $^7\Sigma_g^+$. In these states there are three 4s electrons, or a bond order of one half. These states also have long bond lengths, perhaps because of the 4s repulsion, which favor one-electron bonds. Such one-electron bonds (ie. one electron per bond orbital as in H_2^+, a bond order of one half) and are favored at long R. These one-electron bonds naturally retain the atomic high spin coupling to maximize the exchange interaction.

The strengths of the nd bonds are determined largely by overlap considerations. Since the relative overlaps of nd orbitals are $nd\sigma \approx nd\pi > nd\delta$, the $nd\sigma$ and $nd\pi$ orbitals are filled before the $nd\delta$ orbitals. For the first transition row, the $d\delta$ overlap is sufficiently small that two-electron $d\delta$ bonds do not contribute strongly to the the binding. For example V_2 has both $d\sigma$ and $d\pi$ two-electron bonds and two $d\delta$ one-electron bonds. In Cr_2 where the two additional electrons are added to the $d\delta$ orbital, instead of increased binding, the D_e is smaller for Cr_2 than V_2. This arises because the small overlap of the $d\delta$ orbitals leads to such weak bonds that they do not compensate for the atomic d-d exchange terms which are lost to form the bond. The loss of these atomic d-d exchange terms is quite important in describing weak bonds. The problems in treating Cr_2 correctly are related to this balance of weak two electron $d\delta$ bonds and the atomic d-d exchange interactions. Since this problem is not present in the other dimers considered, our CASSCF treatment fails only for Cr_2.

There are several differences between the first and second transition row: i)$\langle r_{5s}\rangle/\langle r_{4d}\rangle$ is smaller than $\langle r_{4s}\rangle/\langle r_{3d}\rangle$ for comparable loca-

tions in the first row ii) the exchange interactions are smaller for 4d than for 3d and iii) the $5s^2 4d^m \rightarrow 5s^1 4d^{m+1}$ excitation energy is smaller than the $4s^2 3d^m \rightarrow 4s^1 3d^{m+1}$ excitation energy. These features lead to stronger 4d bonding than 3d, with a notable increase in the strength of the dδ bond and a reduced significance of the mixed asymptote. There are several examples of these changes. Y_2 has a low-lying $^1\Sigma_g^+$ state, which is a very likely candidate for the ground state, arising from $5s^1 4d^2 + 5s^1 4d^2$. Mo_2 has a larger D_e than Cr_2 and the CASSCF treatment is now able to describe this bonding. Nb_2 has a low-lying $^3\Delta_g$ state ($4d\sigma_g^1 4d\pi_u^4 4d\delta_g^3$) which arises by moving a 4dσ electron into a 4dδ orbital, while the corresponding state is 0.92 eV up for V_2

REFERENCES

1. W. Weltner, Jr., and R.J. VanZee, Ann. Rev. Phys. Chem., 35, 291 (1984).
2. See articles in "Recent Developments and Applications of Multi Configuration Hartree-Fock Methods" NRCC Proceedings No. 10, M. Dupuis, editor, NRCC, 1981.
3. P. E. M. Siegbahn, A. Heiberg, B. O. Roos, and B. Levy, Physica Scripta, 21, 323 (1980); B. O. Roos, P. R. Taylor, P. E. M. Siegbahn, Chem. Phys, 48, 157 (1980); P. E. M. Siegbahn, J. Almlof, A. Heiberg, and B. O. Roos, J. Chem. Phys., 74, 2384 (1981).
4. H. Lischka, R. Shepard, F.B. Brown, and I. Shavitt, Int. J. Quantum Chem. Symp. 15, 91 (1981); P. E. M. Siegbahn, J. Chem. Phys, 72, 1647 (1980); B. Liu and M. Yoshimine, J. Chem. Phys., 74, 612 (1981);P. Saxe, D. Fox, H.F. Schaefer III, and N.C. Handy, J. Chem. Phys., 77, 5584(1982).
5. W.A. Goddard, III, T.H. Dunning, Jr., W.J. Hunt, and P.J. Hay, Acc. Chem. Res., 6, 368 (1973);T.H. Dunning, Jr., in "Advanced Theories and Computational Approaches to the Electronic Structure of Molecules", edited by C.E. Dykstra, Reidel Publishing(1983), p.67
6. M.R.A. Blomberg, U.B. Brandemark, and P.E.M. Siegbahn, preprint communicated to authors
7. A.E. Stevens, C.S. Feigerle, and W.C. Lineberger, J. Amer. Chem. Soc., 104, 5026 (1982).
8. M.M. Goodgame and W.A. Goddard III, Phys. Rev. Lett., 48, 135 (1982); J. Phys. Chem. 85, 215 (1981)
9. S.P. Walch, C.W. Bauschlicher, Jr., B.O. Roos, and C.J. Nelin, Chem. Phys. Lett., 103, 175 (1983).
10. I. Shim and K. Gingerich, J. Chem. Phys., 77, 2490 (1982); J. Chem. Phys. 78, 5693 (1983)
11. F.A. Cotton and I. Shim, J. Amer. Chem. Soc., 104, 7025 (1982).
12. S.P. Walch, to be published.
13. G.P. Das and R.L. Jaffe, Chem. Phys. Lett., 109, 206 (1984).
14. M.M. Goodgame and W.A. Goddard III, paper presented at the Sixth West Coast Theory Conference, Los Alamos, New Mexico, April 1984.
15. The experimental atomic separations are taken from ref.16, while the orbital sizes are from numerical Hartree-Fock calculations.

16. C. E. Moore, Atomic energy levels, Natl. Bur. Stand. (US) circ. 467 (1949).

17. S.P.Walch and C.W. Bauschlicher, Jr., Chem. Phys. Lett., 94, 290 (1983).

18. R.L.Martin and P.J.Hay, J. Chem. Phys., 75, 4539 (1981).

19. P.J. Hay, J. Chem. Phys., 66, 4377 (1977).

20. A.J.H. Wachters, J. Chem. Phys., 58, 4452 (1973).

21. A.D. McLean and B. Liu, Chem. Phys. Lett., 101, 144 (1983).

22. S. Huzinaga, J. Chem. Phys., 66, 4245 (1977).

23. S.P. Walch, C.W. Bauschlicher, Jr., and C.J. Nelin, J. Chem. Phys., 79, 3600 (1983).

24. J. Almlof, MOLECULE, a gaussian integral program.

25. P.E.M. Seigbahn, C.W. Bauschlicher, Jr., B. Roos, A. Hieberg, P. R. Taylor, and J. Almof, SWEDEN, a vectorized SCF MCSCF direct CI.

26. R.C. Raffenetti, BIGGMOLI, Program No. 328, Quantum Chemistry Program Exchange, Indiana University, Bloomington(1977), with modifications to allow use of the full D_{2h} symmetry.

27. J. Drowart and R.E. Honig, J. Phys. Chem., 61, 6801 (1957).

28. L.B. Knight, R.J. VanZee, and W. Weltner, Jr. , Chem. Phys. Lett., 94, 296 (1983).

29. D.P. DiLella, W. Limm, R.H. Lipson, M. Moskovits, and K.V. Taylor, J. Chem. Phys., 77, 5263 (1982).

30. S.P. Walch and C.W. Bauschlicher, Jr., J. Chem. Phys., 79, 3590 (1983).

31. A. Kant and S.H.Lin, J. Chem. Phys., 51, 1644 (1965).

32. P.R.R. Langridge-Smith, M.D. Morse, G.P. Hansen, R.E. Smalley, and A.J. Merer, J. Chem. Phys., 80 , 593 (1984).

33. A. Merer, private communication.

34. A. Kant and B. Strauss, J. Chem. Phys., 45, 3161 (1966).

35. S.P. Walch and C.W. Bauschlicher, Jr., J. Chem. Phys., 78, 4597(1983)

36. R. J. Van Zee and W. Weltner, Jr., Chem. Phys. Lett., 107 , 173 (1984).

37. C.W. Bauschlicher, Jr., S.P. Walch, and P.E.M. Siegbahn, J. Chem. Phys., 76, 6015 (1982).

38. C.W. Bauschlicher, Jr., S.P. Walch, and P.E.M. Siegbahn, J. Chem. Phys., 78, 3347 (1983).

39. L. Pauling, J. Chem. Phys., 78, 3346 (1983).

40. H. Partridge, C. W. Bauschlicher, Jr., S. P. Walch, and B. Liu, J. Chem. Phys., 79, 1866 (1983).

41. R. Martin, J. Chem. Phys., 78, 5240 (1983).

42. B. Laskowski, C. W. Bauschlicher, Jr., and S.R. Langhoff, to be published.

43. R. Martin and W. Werner, private communication.

44. C. W. Bauschlicher, Jr., Chem. Phys. Letters, 97, 204 (1983).

45. L. B. Knight, R. W. Woodward, R. J. Van Zee, and W. Weltner, Jr., J. Chem. Phys., 79, 5820 (1983).

46. R.E. Smalley, Paper Presented at the 1984 ACS Annual Meeting, Philadelphia, Pennsylvania, August 1984.

47. Y. M. Efremov, A. N. Samoilova, V. B. Kozkukhowsky, and L. V. Gurvich, J. Mol. Spect., 73, 430 (1978).

48. S. K. Gupta, R. M. Atkins, and K. A. Gingerich Inorg. Chem., 17, 3211 (1978).

49. D.L. Michalopoulos, M.E. Geusic, S.G. Hansen, D.E. Powers and R.E. Smalley, J. Phys. Chem., 86, 3914 (1982).

50. V.E. Bondybey and J.H. English, Chem. Phys. Lett., 94, 443 (1983).

51. S.J. Riley, E.K. Parks, L.G. Pobo, and S. Wexler, J. Chem. Phys., 79, 2577 (1983).

52. P. E. M. Siegbahn, Int. J. Quantum Chem., 23, 1869 (1983).

Table Ia. Relative orbital sizes and excitation energies for first row transition metal atoms. The orbital expectation values are taken from Numerical Hartree-Fock calculation, while the excitation energies are taken from experiment.

Atom	$\langle r_{4s} \rangle / \langle r_{3d} \rangle$	$4s^2 3d^m \rightarrow 4s^1 3d^{m+1}$	$4s^2 3d^m \rightarrow 3d^{m+2}$
Sc	2.03	1.43	4.19
Ti	2.32	0.81	3.35
V	2.51	0.25	2.47
Cr	2.69	-1.00	3.40
Mn	2.81	2.14	5.59
Fe	2.95	0.87	4.07
Co	3.08	0.42	3.36
Ni	3.22	-0.03	1.71
Cu	3.36	-1.49	

Table Ib. Relative orbital sizes and excitation energies for second row transition metal atoms. The orbital expectation values are taken from Numerical Hartree-Fock calculation, while the excitation energies are taken from experiment.

Atom	$\langle r_{5s} \rangle / \langle r_{4d} \rangle$	$5s^2 4d^m \rightarrow 5s^1 4d^{m+1}$	$5s^2 4d^m \rightarrow 4d^{m+2}$
Y	1.61	1.36	3.63
Zr	1.79	0.59	2.66
Nb	1.92	-0.18	1.14
Mo	2.05	-1.47	1.71
Tc	2.16	0.41	
Ru	2.29	-0.87	0.22
Rh	2.42	-1.63	-1.29
Pd	2.54	-2.43	-3.38
Ag	2.67	-3.97	

Table II. Calculated spectroscopic constants for first row transition metal dimers

Molecule	R_e (A)	ω_e (cm^{-1})	D_e (eV)	T_e (eV)
Sc_2 $^5\Sigma_u^-$				
CI	2.79	184.	0.44	
Exp.		238.9[a]	1.13[b]	
Ti_2 $^1\Sigma_g^+$				
CASSCF	1.97	436.	0.37	
CI	1.97	438.	1.94	0.40
Exp.		407.9[a]	2.91[c]	
Ti_2 $^7\Sigma_u^+$				
CI	2.63	205.	1.53	0.00
V_2 $^3\Sigma_g^-$				
CASSCF	1.76	564.	0.60	0.00
Exp.	1.76[d]	537.5[a]	2.29[d], 2.97[c]	
V_2 $^1\Gamma_g$				
CASSCF	1.80	486.	0.58	0.02
V_2 $^3\Delta_g$				
CASSCF	1.77	413.	-0.32	0.92
Cr_2 $^1\Sigma_g^+$				
CASSCF			-1.4	
Exp.	1.68[e]	480.[a]	1.56[f]	

[a] Ref. 29
[b] Ref. 27
[c] Ref. 31
[d] Ref. 32
[e] Ref. 49-51
[f] Ref. 34

Table III. Calculated spectroscopic constants for the TiV molecule

State	R_e (Å)	ω_e (cm^{-1})	D_e (eV)[a]
$^4\Sigma^-$	1.86	495.	0.80
$^4\Pi$	1.95	410.	0.15
$^2\Delta$	1.89	472.	0.43

[a] Calculated with respect to $Ti(4s^1 3d^3)$ + $V(4s^1 3d^4)$.

Table IV. Calculated spectroscopic constants for second row transition metal dimers

Molecule	R_e (A)	ω_e (cm^{-1})	D_e (eV)	T_e (eV)
Y_2 $^5\Sigma_u^-$				
CI	3.03	171.	2.44	0.00
Y_2 $^1\Sigma_g^+$				
CASSCF	2.73	205.	1.74	
CI	2.74	206.	2.93	0.87
Nb_2 $^3\Sigma_g^-$				
CASSCF	2.10	448.	2.24	0.00
Nb_2 $^1\Gamma_g$				
CASSCF	2.11	427.	2.15	0.09
Nb_2 $^3\Delta_g$				
CASSCF	2.01	501.	2.12	0.12
Nb_2 $^3\Phi_g$				
CASSCF	2.19	340.	1.28	0.96
Mo_2 $^1\Sigma_g^+$				
CASSCF	1.99	399.	0.77	
Exp.	1.93[a]	477.[a]	4.2[b]	

[a] Ref. 47
[b] Ref. 48

Figure Captions.

Fig. 1. Calculated CASSCF/CI potential curves for selected states of Sc_2.

Fig. 2. Calculated CASSCF potential curves for selected states of V_2.

Fig. 3. Calculated potential curves for the $^1\Sigma_g^+$ state of Cr_2. The curve labeled CASSCF + 3d′ includes an estimate of 3d′ correlation from the extended CASSCF calculations of Walch (Ref. 12);while the curve labeled CASSCF + 3d′ + 4p(Est.) also includes an estimate of the 4p correlation based on extended CASSCF calculations on Ti_2 (Ref 12.). Because the correlation contributions are obtained by summing individual energy contributions the effect of 3d′ is expected to be significantly overestimated (see text). Thus, we expect that a CASSCF calculation in which all the 3d′ orbitals were added simultaneously would show a much reduced binding energy contribution due to 3d′ leading to a potential curve with a more distinct shoulder than the CASSCF curve but no well.

Fig. 4. Calculated CASSCF potential curves for selected states of TiV.

Fig. 5. Calculated CASSCF/CI potential curves for selected states of Y_2.

Fig. 6. Calculated CASSCF potential curves for selected states of Nb_2.

Sc_2 CASSCF/CI

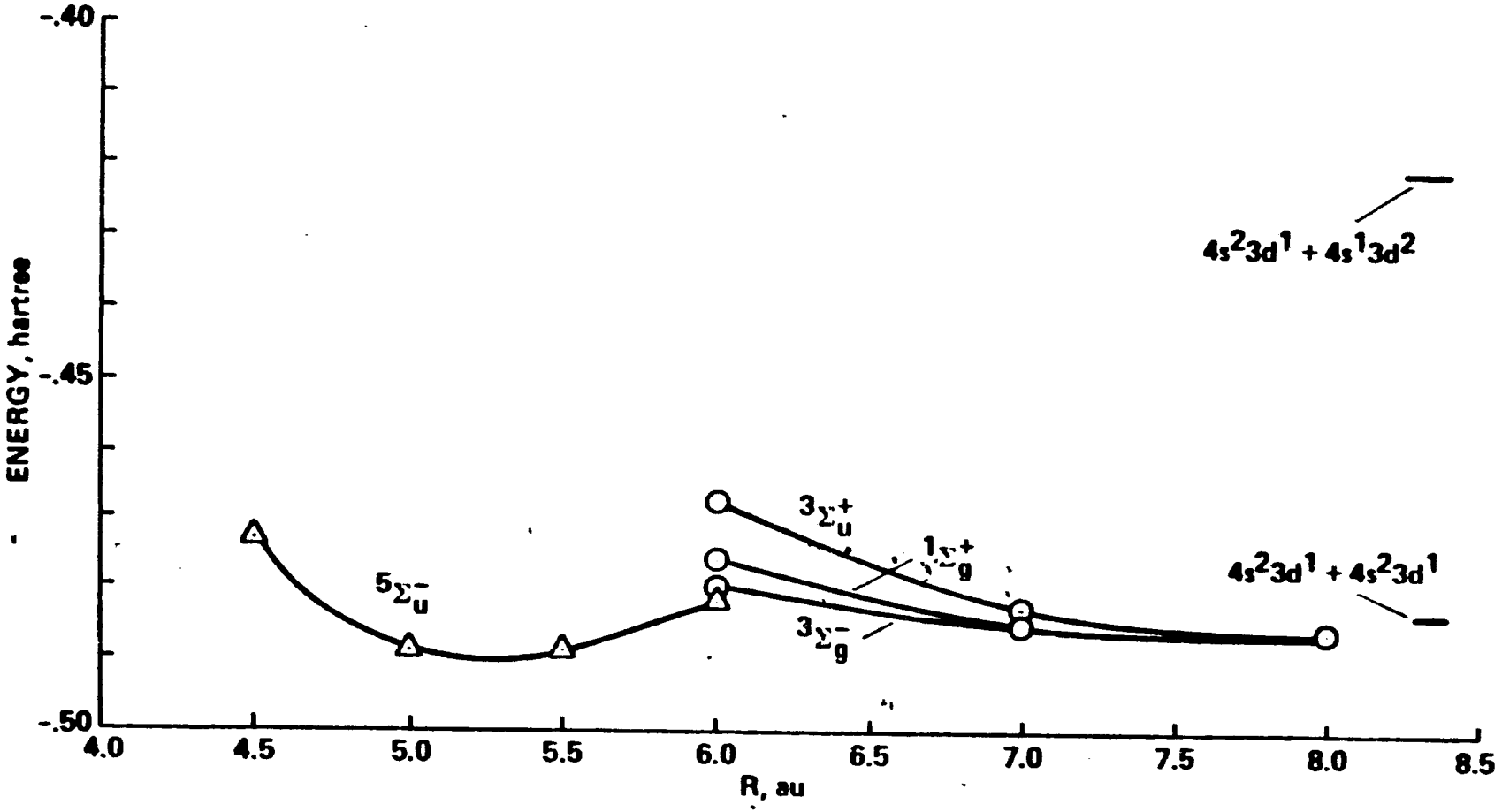

Fig. 2

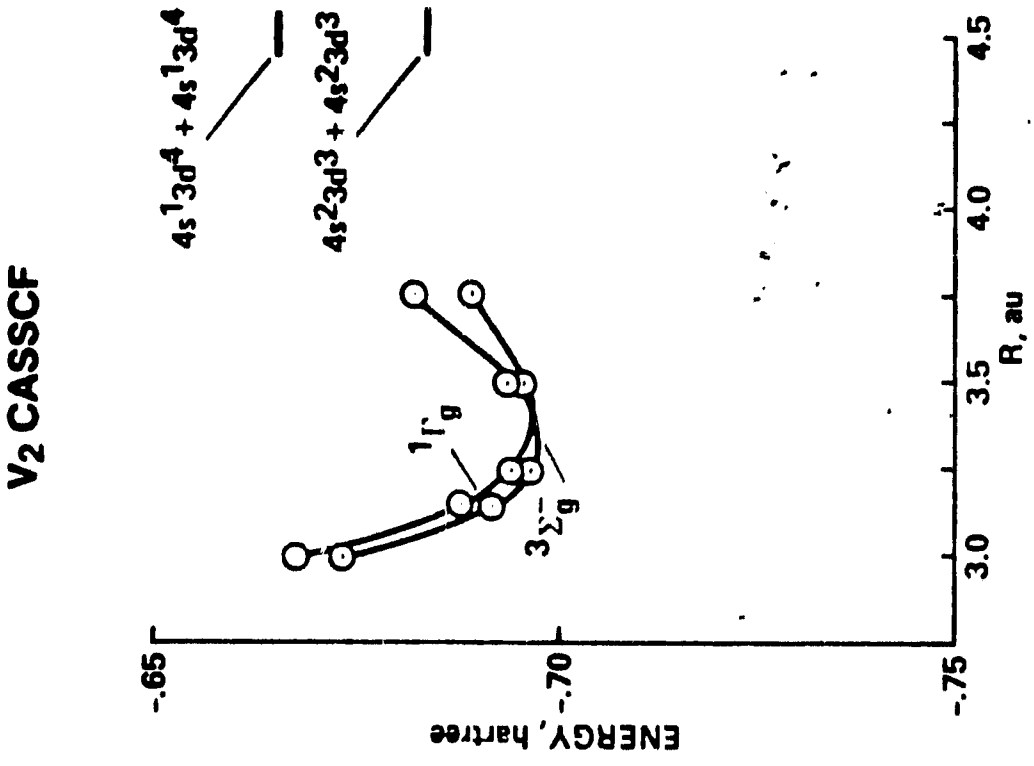
V2 CASSCF
4s13d4 + 4s13d4
4s23d3 + 4s23d3
1Γg
3Σ-g
-.65
-.70
-.75
ENERGY, hartree
3.0
3.5
4.0
4.5
R, au

Cr_2 CASSCF

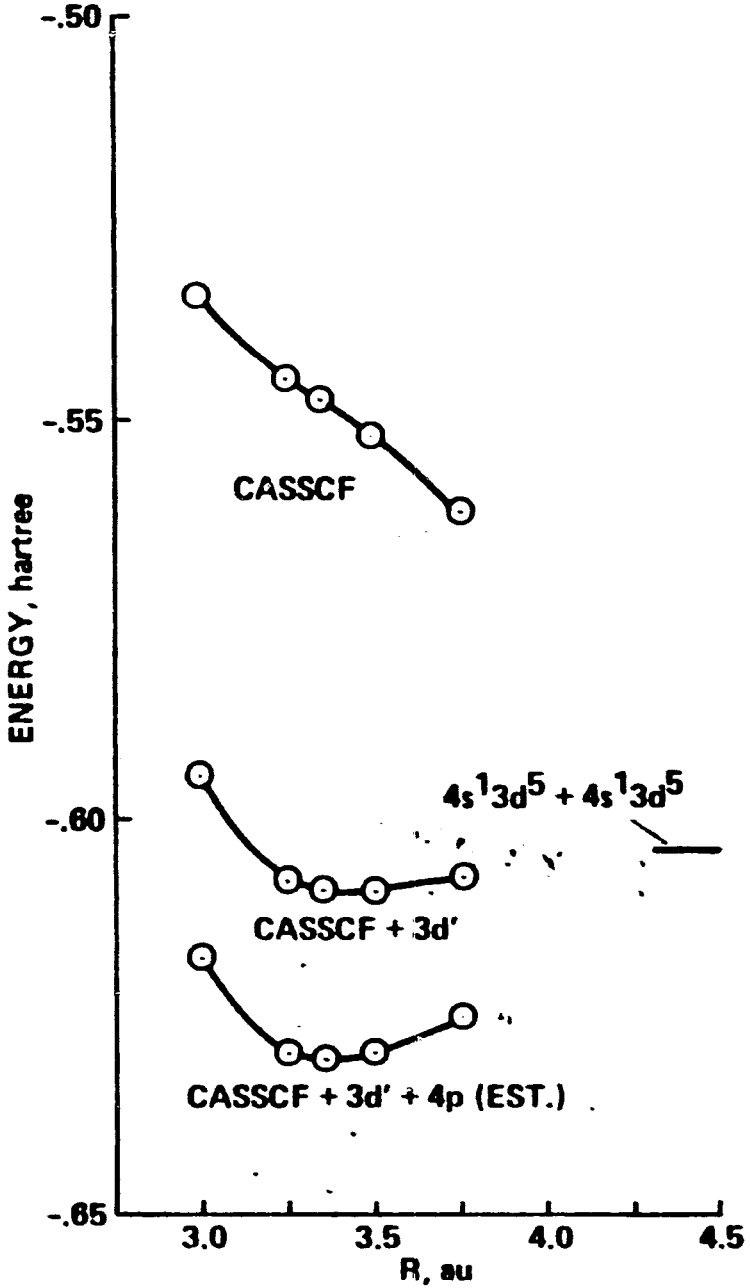
-.50
-.55
-.60
-.65
ENERGY, hartree
CASSCF
$4s^1 3d^5 + 4s^1 3d^5$
CASSCF + 3d'
CASSCF + 3d' + 4p (EST.)
3.0
3.5
4.0
4.5
R, au

Fig. 4

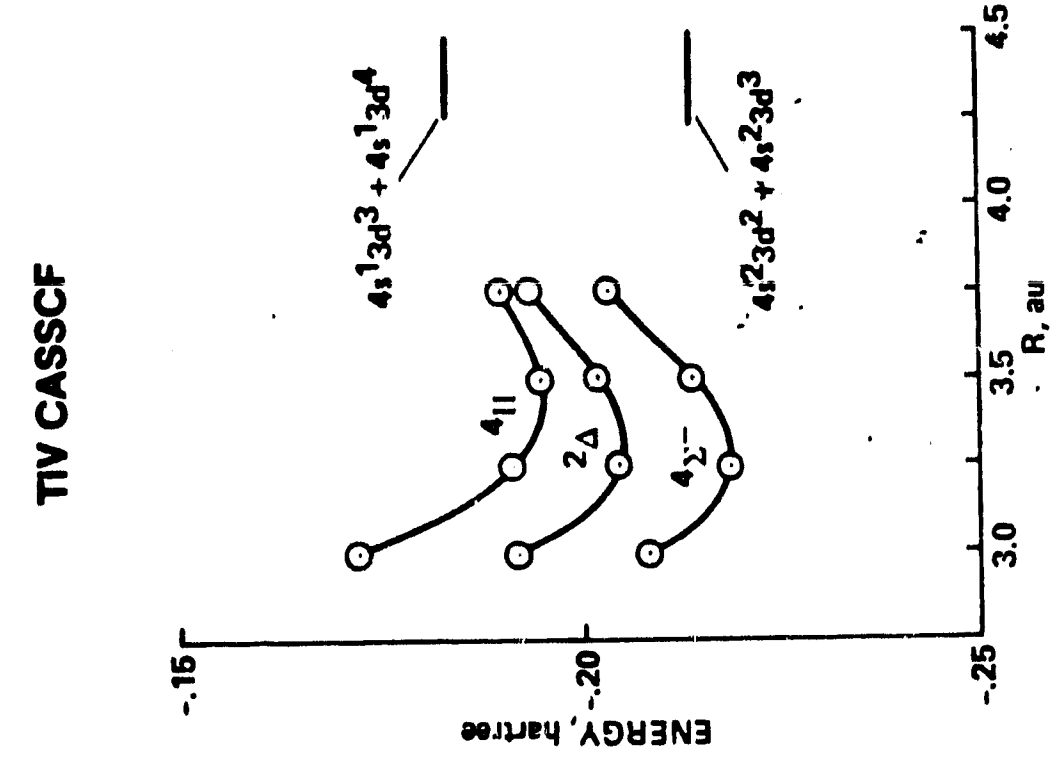
TiV CASSCF
$4s^13d^3 + 4s^13d^4$
$4s^23d^2 + 4s^23d^3$
$^4\Pi$
$^2\Delta$
$^4\Sigma^-$
-.15
-.20
-.25
ENERGY, hartree
3.0
3.5
4.0
4.5
R, au

Y_2 CASSCF/CI

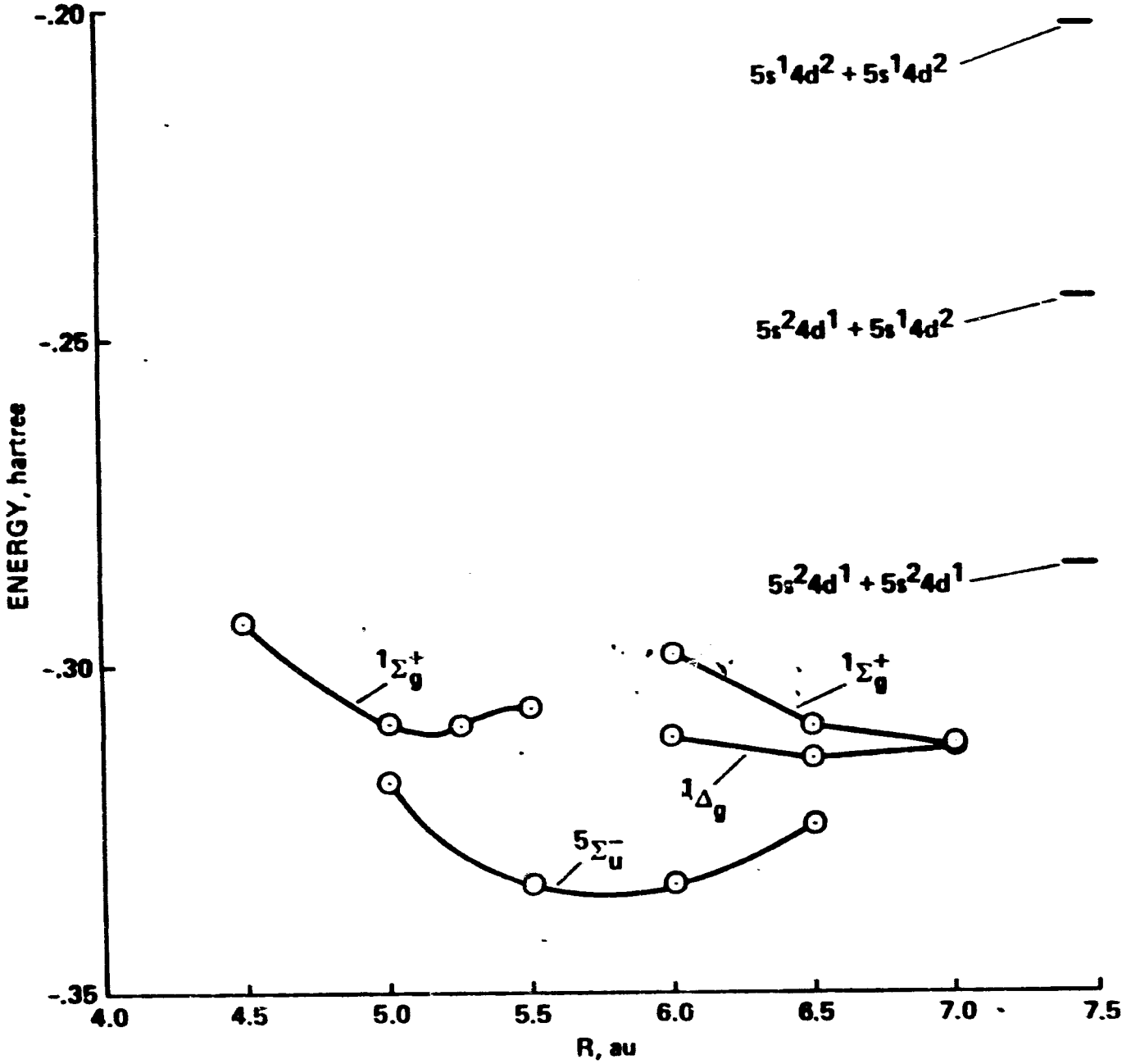

Fig. 5

Fig. 6

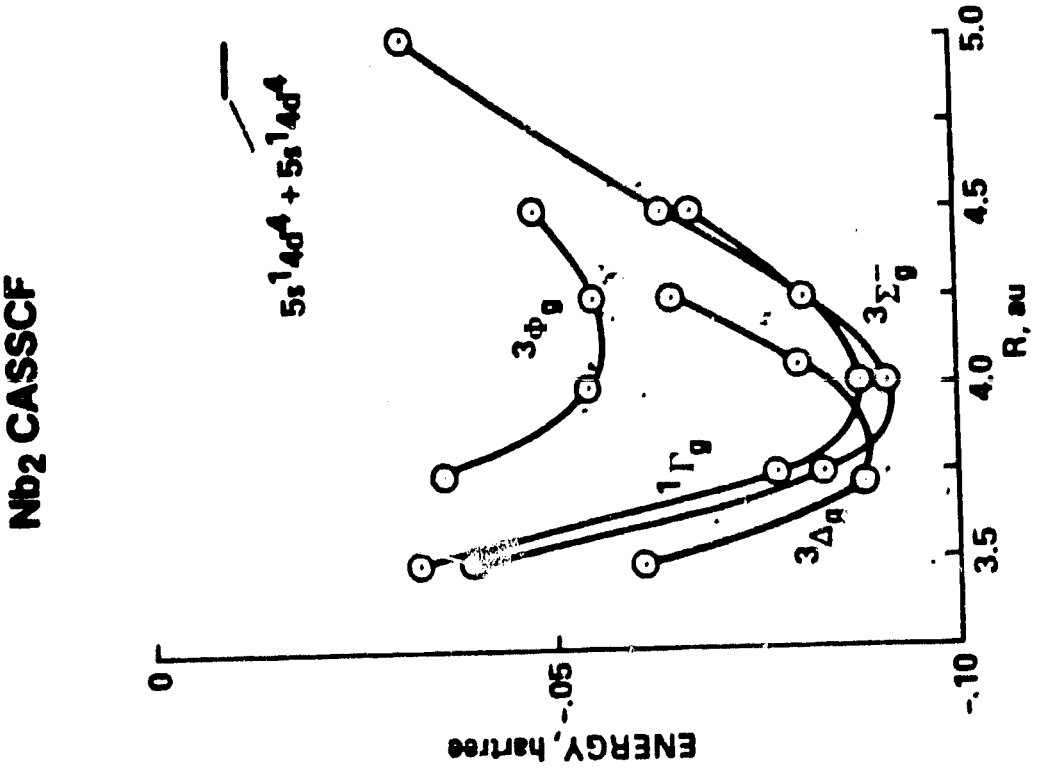
Nb2 CASSCF
5s14d4 + 5s14d4
3Φg
1Γg
3Δg
3Σg−
ENERGY, hartree
0
-.05
-.10
3.5
4.0
4.5
5.0
R, au